Journal of Magnetic Resonance 206 (2010) 255–263

Contents lists available at ScienceDirect

Journal of Magnetic Resonance

journal homepage: www.elsevier.com/locate/jmr

Frequency-swept pulse sequences for ^{19}F heteronuclear spin decoupling in solid-state NMR

C. Vinod Chandran [a], P.K. Madhu [b], Philip Wormald [c], Thomas Bräuniger [a,*]

[a] Max-Planck-Institute of Solid-State Research, Heisenbergstr. 1, 70569 Stuttgart, Germany
[b] Department of Chemical Sciences, Tata Institute of Fundamental Research, Homi Bhabha Road, Colaba, Mumbai 400 005, India
[c] School of Chemistry, University of St. Andrews, Purdie Building, St. Andrews KY16 9ST, Scotland, United Kingdom

ARTICLE INFO

Article history:
Received 9 June 2010
Revised 19 July 2010
Available online 1 August 2010

Keywords:
Solid-state NMR
^{19}F heteronuclear dipolar decoupling
SW$_f$-TPPM
SW$_f$-SPINAL

ABSTRACT

Heteronuclear spin decoupling pulse sequences in solid-state NMR have mostly been designed and applied for irradiating ^{1}H as the abundant nucleus. Here, a systematic comparison of different methods for decoupling ^{19}F in rigid organic solids is presented, with a special emphasis on the recently introduced frequency-swept sequences. An extensive series of NMR experiments at different MAS frequencies was conducted on fluorinated model compounds, in combination with large sets of numerical simulations. From both experiments and simulations it can be concluded that the frequency-swept sequences SW$_f$-TPPM and SW$_f$-SPINAL deliver better and more robust spin decoupling than the original sequences SPINAL and TPPM. Whereas the existence of a large chemical shift anisotropy and isotropic shift dispersion for ^{19}F does compromise the decoupling efficiency, the relative performance hierarchy of the sequences remains unaffected. Therefore, in the context of rigid organic solids under moderate MAS frequencies, the performance trends observed for ^{19}F decoupling are very similar to those observed for ^{1}H decoupling.

1. Introduction

Application of heteronuclear spin decoupling provides significant assistance in improving the resolution of solid-state NMR spectra [1,2]. Along with magic angle spinning (MAS), it helps to reduce the line broadening of NMR spectral lines due to dipolar interactions. Initially, continuous wave (CW) irradiation [3–5] was used on the abundant spins (such as ^{1}H), facilitating an improvement in resolution of the signals from the rare spin (such as ^{13}C). Bennett et al. [6] were the first to introduce a multi-pulse sequence for spin decoupling in solid-state NMR, namely Two Pulse Phase Modulation (TPPM), which resulted in much improved decoupling performance compared to CW irradiation. The TPPM sequence consists of repeating units of two RF pulses with alternating phases $\tau_{(+\phi)}\tau_{(-\phi)}$, where τ is the pulse duration (with a flip angle usually between 160° and 180°) and ϕ is the phase angle. Although the sequence has been used widely since its invention, it shows considerable sensitivity towards changes in NMR parameters like flip angle and phase angle. An alternative was suggested by Fung et al., with the Small Phase Incremental ALteration (SPINAL) sequence [7], which includes phase increments within a certain train of pulses Q of the form $\tau_{(+\phi)}\tau_{(-\phi)}\tau_{(\phi+\alpha)}\tau_{(-\phi-\alpha)}\tau_{(\phi+\beta)}\tau_{(-\phi-\beta)}\tau_{(\phi+\alpha)}\tau_{(-\phi-\alpha)}$. The most efficient phase increments usually are $\alpha = 5°$ and $\beta = 10°$. A super-cycled sequence with eight such blocks of pulses arranged as $Q\overline{Q}Q\ \overline{Q}Q\overline{Q}$, thus constitutes a SPINAL-64 sequence. Although SPINAL-64 was initially designed for liquid crystal NMR, it also works well for crystalline solids and has been shown to outperform TPPM in many instances [7–9]. Several other multi-pulse decoupling sequences were introduced later. Detken et al. published a scheme with repeating units of two rotor-synchronised pulses with 180° phase shift, known as X-inverse-X (XiX) [10], which was based on an earlier suggestion by Tekely [11]. Other approaches for efficient heteronuclear decoupling include symmetry-based sequences [12,13], Cosine Modulated (CM) TPPM [14], Hahn-Echo trains [15] and Phase-Wiggled (PW) TPPM [16]. A theoretical analysis of phase-modulated sequences was presented recently by Ernst and co-workers [17].

A new approach, SW$_f$-TPPM [18–23], was introduced recently, and was found to have better decoupling efficiency than both TPPM and SPINAL. In SW$_f$-TPPM, the durations of the pulse pairs are changed in a controlled manner over a block of typically 11 pulse pairs, by multiplying the pulse durations with a series of factors which range from values below unity to values above unity in a symmetrical manner (see Fig. 1). The change of pulse duration of the phase-modulated pulse pairs leads to a change (a 'sweep') of the frequency generated by the phase modulation, as can be shown by Fourier transformation [18,24]. The sequence of pulse multiplication factors defines a *sweep profile*. Initially, SW$_f$-TPPM was introduced with a tangential sweep profile [18]. Later linear sweeps

* Corresponding author. Fax: +49 711 689 1502.
E-mail address: T.Braeuniger@fkf.mpg.de (T. Bräuniger).

1090-7807/$ - see front matter © 2010 Elsevier Inc. All rights reserved.
doi:10.1016/j.jmr.2010.07.018

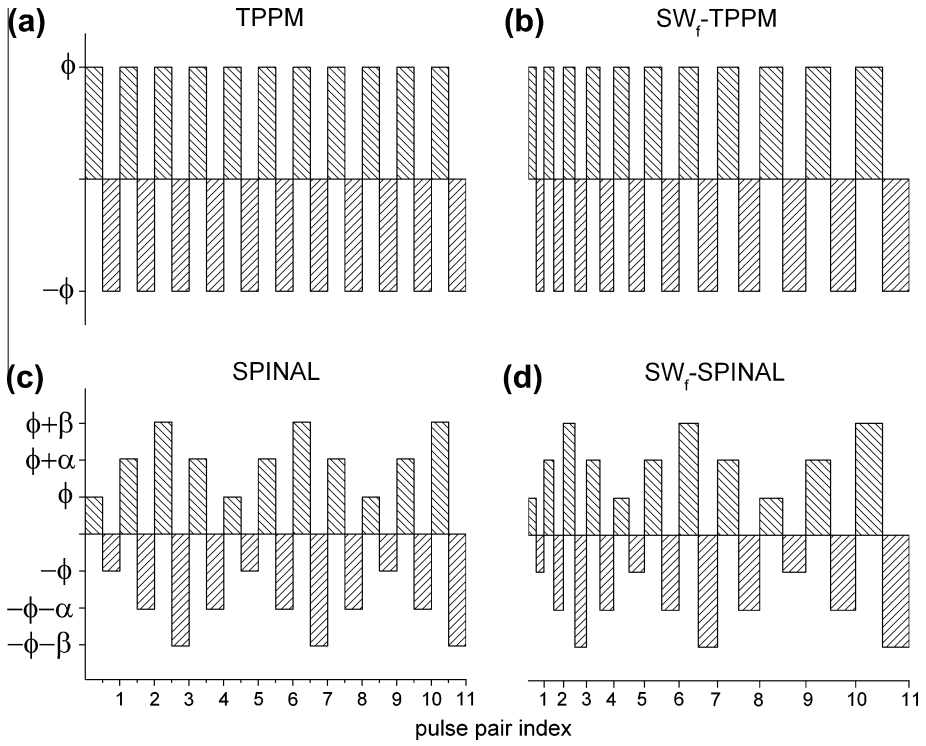

Fig. 1. Schematic representation of the decoupling sequences (a) TPPM, (b) SW$_f$-TPPM, (c) SPINAL, and (d) SW$_f$-SPINAL.

were found to be equally good-performing, with one optimizable parameter less than the tangential sweeps, making implementation and optimization easier [20,22]. The SW$_f$-TPPM method was found useful for dipolar decoupling in many systems including liquid crystals [19], crystalline organic solids [18,20,22,23] and inorganic materials with quadrupolar nuclei [21,25]. The decoupling performance of SW$_f$-TPPM methods was also analysed using bimodal Floquet theory [20]. In SW$_f$-TPPM, only the pulse duration is modulated. It is however possible to simultaneously modulate both pulse durations and phases, leading to doubly modulated sequences. The phase modulated version of SW$_f$-TPPM is known as SW$_{fp}$-TPPM [26] and has been shown to add a few percent to the performance of SW$_f$-TPPM. Another doubly modulated sequence is the frequency-swept SPINAL sequence, named SW$_f$-SPINAL [27]. It was found that incorporation of a pulse duration sweep generally improves the decoupling performance of SPINAL, although not always to the quality of SW$_f$- or SW$_{fp}$-TPPM.

A major cause of line broadening in solid-state NMR is the dipolar interaction. For nuclei with high gyromagnetic ratio and/or in close proximity, this interaction is only scaled down, but not fully eliminated at moderate MAS frequencies [28]. Another reason for line broadening are chemical shift effects. The full chemical shift Hamiltonian of a spin system in an external magnetic field $\vec{B}_0$ is given by:

$$\widehat{\mathscr{H}}_{CS} = -\gamma \vec{B}_0 \cdot \delta \cdot \vec{B} \tag{1}$$

Here δ is the chemical shift tensor, the principal values of which determine the isotropic value of the chemical shift:

$$\delta_{iso} = \frac{1}{3}(\delta_{11} + \delta_{22} + \delta_{33}) \tag{2}$$

Setting the decoupler frequency exactly on the abundant spin resonance is an easy procedure in the case of narrow spectral lines, but is not so obvious for broad and featureless lines often encountered in solid-state NMR. Similarly, for a sample with a spread of isotropic chemical shifts for the abundant nuclei, *on-resonance* conditions cannot be met simultaneously. This effect of isotropic shift spread may be termed *isotropic dispersion* [29], and here we designate the magnitude of this dispersion by $d\delta_{iso}$. In solids, an additional difficulty arises because of the orientation-dependent chemical shift anisotropy (CSA), which can be gauged by the quantity

$$\Delta\delta = (\delta_{33} - \delta_{iso}) \tag{3}$$

with an associated asymmetry parameter,

$$\eta = \frac{(\delta_{22} - \delta_{11})}{\Delta\delta} \tag{4}$$

This standard convention is valid for shielding tensors with the condition $|\delta_{33} - \delta_{iso}| \geqslant |\delta_{22} - \delta_{iso}| \geqslant |\delta_{11} - \delta_{iso}|$ according to the IUPAC rules [30]. In principle, the chemical shift anisotropy (CSA) may be averaged out by MAS, if the spinning speed exceeds the magnitude of the CSA interaction. For ^{1}H, both $d\delta_{iso}$ and $\Delta\delta$ are comparatively small, namely up to tens of ppm. The situation is different for the nucleus ^{19}F, which is otherwise – in terms of NMR response – very similar to ^{1}H: ^{19}F possesses spin $I = 1/2$, a natural abundance of 100%, and a gyromagnetic ratio close to that of ^{1}H. But even when placed in a similar chemical environment, the chemical shift effects experienced by ^{19}F are much larger than those of ^{1}H, due to a larger electron cloud. As may be seen from Table 1, the dispersion of ^{19}F isotropic shifts $d\delta_{iso}$ tends to be much larger than that of protons, whereas the magnitude of $\Delta\delta$ of ^{19}F may reach hundreds of ppm. Under MAS conditions, $d\delta_{iso}$ will be not affected at all, whereas for slow to moderate spinning speeds, $\Delta\delta$ will not be averaged completely. This adds to the challenge of performing efficient spin decoupling for ^{19}F nuclei. This raises the question of how spin decoupling techniques, usually designed and tested for ^{1}H decoupling, perform when applied to ^{19}F.

The necessity for efficient decoupling of ^{19}F occurs frequently in solid-state NMR, as fluorine is present in many important materials like polymers, minerals and ceramics. Consequently, a large number of examples may be found in the literature where a rare spin

Table 1
Comparison of isotropic chemical shift ($\delta_{iso} = \frac{1}{3}[\delta_{11} + \delta_{22} + \delta_{33}]$) and the chemical shift anisotropy ($\Delta\delta = \delta_{33} - \delta_{iso}$) for ^{1}H and ^{19}F nuclei in similar chemical environments. The acquisition temperatures (T) and the corresponding references from which the data have been taken are also listed.

Compound	^{1}H				Compound	^{19}F			
	δ_{iso}/ppm	$\Delta\delta$/ppm	T/K	Ref.		δ_{iso}/ppm	$\Delta\delta$/ppm	T/K	Ref.
$CHCl_3$	24	8.6	RT[a]	[31]	$CFCl_3$	190	51	RT[a]	[32]
NH_3	31.2	15.61	–	[33,34]	NF_3	74.9	390.0	RT[b]	[35,36]
C_6H_6	7	−5.3	263	[37]	C_6F_6	0.33	149.5	201	[38]
1,3,5-tribromobenzene	–	−6.95	–	[39]	1,3,5-trifluoro-tribromobenzene	81.0	−112.0	–	[39]
4,4′-difluorobiphenyl	−6.5, −7.5	5.0, 2.0	RT	[40]	4,4′-difluorobiphenyl	−52.5	51.77	RT	[40]
2,6-dichloro 4-fluorophenol	7.04	4.45	RT	[41]	2,6-dichloro 4-fluorophenol	−127.02	87.86	RT	[41]

[a] Determined from solution in liquid-crystalline media.
[b] Determined from molecules trapped in clathrates.

has been observed under ^{19}F decoupling [42–62]. Whereas in many cases, only CW decoupling has been used [42–53], there is also evidence of application of multi-pulse techniques. In analogy to the results obtained for ^{1}H, it was attempted to improve spectral resolution by decoupling ^{19}F using TPPM [54–58], SPINAL [59,60] and also XiX [61,62]. We are however not aware of any work where the respective performances of different ^{19}F decoupling techniques have been systematically compared. Therefore, in the present work, a systematic comparison of ^{19}F-decoupling efficiencies of different composite pulse decoupling sequences performed in rigid perfluoro-organic systems is presented, with a special emphasis given to the new frequency-swept sequences. TPPM, SPINAL, SW$_f$-TPPM and SW$_f$-SPINAL (Fig. 1) are the methods which are being compared, in decoupling experiments conducted on potassium nonafluoro-1-butanesulfonate (NFBS-K) and sodium pentafluoropropionate (PFP-Na). These model compounds may be classified as "rigid organic solids" on the NMR time scale. Also, the rare spin ^{13}C is observed in the presence of ^{19}F only, and we restrict ourselves to such systems in the work presented here. Another experimentally important situation is the simultaneous presence of ^{1}H and ^{19}F. For isolated (or very dilute) H–X–F pairs, offset-robust decoupling on ^{1}H only may be sufficient for good resolution [63]. For systems that are abundant in both ^{1}H and ^{19}F, however, triple resonance experiments need to be performed in order to decouple both nuclides [64–71]. We have also not looked at polymers in this work, as these are conceptually different from rigid organic solids, and are known to respond differently to *RF* decoupling [70–76]. Since all the experiments were performed at comparatively moderate spinning speeds (below 20 kHz), XiX [10] and the recently suggested PISSARRO [77,78] were not considered, as they work well only at high spinning speeds. We also conducted SPINEVOLUTION [79] numerical simulations to evaluate the performance of the various decoupling schemes. Both in experiment and in simulation, the frequency-swept sequences always outperformed TPPM and SPINAL by a consistent margin, with an enhanced robustness towards parameter changes.

2. Experimental

Potassium nonafluoro-1-butanesulfonate (NFBS-K, Sigma Aldrich) and sodium pentafluoropropionate (PFP-Na, Acros Organics) were purchased and used without further purification. The ^{19}F spectrum of NFBS-K in D_2O solution was recorded on a BRUKER AVANCE-II 400 spectrometer. It showed multiplet structures centred at −81.42 ppm for the CF_3 group (δ carbon), and for the CF_2 groups at −115.17 (α), −122.40 (γ), and −126.52 ppm (β). The $^{19}F \rightarrow {}^{13}C$ Cross Polarization Magic Angle Spinning (CPMAS) spectra of NFBS-K and PFP-Na were acquired on a BRUKER AVANCE-II 400 spectrometer, at a ^{13}C Larmor frequency of 100.58 MHz and a ^{19}F Larmor frequency of 376.13 MHz, using a 2.5 mm double channel MAS probe (NMR Service, M. Braun) at different spinning frequencies (10, 15, and 20 kHz). A CP contact time of 5 ms was used for both model compounds with a recycle delay of 5 s for PFP-Na and 7 s for NFBS-K, with 128 transients collected for each spectrum. All decoupling sequences used were coded in the standard BRUKER CPD format and are available from the authors upon request. The parameters governing the decoupling sequences were optimized by sequentially changing pulse durations, phase angles and sweep profiles while searching for the maximum intensity of the ^{13}C signal. More details on optimization may be found in earlier works [22,25,27]. Since the linear and the tangential sweep profiles produced similar decoupling efficiency, only results from the linear profiles are shown in the comparison plots. All the experiments were done at a decoupling field strength of ≈120 kHz.

The performance of the various decoupling schemes was also investigated by SPINEVOLUTION [79] numerical simulations. The spin system under analysis for simulations was a ^{13}C nucleus dipolar-coupled with four ^{19}F nuclei, arranged in a glycinyl backbone structure. All the calculations were run with the ^{19}F–^{19}F homonuclear dipolar interaction enabled and with a range of ^{19}F chemical shielding anisotropies. A line broadening factor of 5 Hz was used for all calculations. MAS frequencies for the simulations of sequences with TPPM and SPINAL basic blocks, were chosen to be 8.0808 kHz and 8.3333 kHz respectively for the 2D plots shown in Fig. 5. This helped to avoid interference effects of the cycle time of the decoupling sequence. A matrix of *RF* strength ν_1 and phase angle ϕ was scanned for each simulation, where ν_1 varies from 80 to 120 kHz in steps of 1 kHz, and ϕ changed from 0° to 30° in 1° step width. The values for the phase settings were identical for TPPM and SW$_f$-TPPM, but for SPINAL and SW$_f$-SPINAL phase increments of $\alpha = 5°$ and $\beta = 10°$ were included.

For ^{19}F decoupling of PFP-Na, the best performing phase angles (ϕ) for TPPM, SW$_f$-TPPM and SW$_f$-SPINAL were found to be 12.5°, but 15° for SPINAL-64. In the case of NFBS-K, the TPPM phase angle was optimized to be 7.5° and for SPINAL-64, SW$_f$-TPPM and SW$_f$-SPINAL, it was 12.5°. For SW$_f$-SPINAL, the sequence SW$_f^{lin}$(32)-SPINAL-32 [27], with a single linear sweep over 32 SPINAL pulses from 0.90 to 1.10 was found to be superior in decoupling of NFBS-K, whereas SW$_f^{lin}$(64)-SPINAL-64 with the identical sweep window (0.90–1.10) proved best for decoupling of PFP-Na. The best sweep for SW$_f$-TPPM was found to be from 0.78 to 1.22 in the case of PFP-Na and from 0.69 to 1.31 for NFBS-K. In all the cases, the flip angles (pulse durations) were optimized experimentally.

3. Results and discussion

3.1. Fluorine decoupling in rigid organic solids

PFP-Na (Fig. 2, top row) and NFBS-K (Fig. 2, bottom row) were used to study the decoupling performance of different decoupling methods. In particular, NFBS-K, with four fluorinated carbon groups, and an isotropic ^{19}F shift dispersion of $d\delta_{iso} \approx 45$ ppm

(see Section 2), appears to be a good candidate for testing decoupling efficiency. As shown in Fig. 2, the frequency-swept TPPM and SPINAL sequences outperform the non-swept sequences by a considerable margin for both samples. PFP-Na shows three resolved carbon resonances, the most de-shielded one being the carbonyl carbon. Since the effect of decoupling on the carbonyl signal intensities is weak, only the difluoromethylene (CF_2) and trifluoromethyl (CF_3) carbon signals of PFP-Na are evaluated in the ^{19}F-decoupled ^{13}C CPMAS spectrum. NFBS-K has four different carbon resonances with the α-carbon (115.3 ppm) being the most de-shielded one, since it is closest to the sulfonate group. Following are the carbon signals of the CF_3 (δ-carbon, 112.5 ppm) and remaining CF_2's (β at 112.5 ppm and γ at 107.1 ppm). The quality of ^{19}F decoupling can be judged from the intensity and the separation of the carbon lines in Fig. 2, with SW_f-TPPM and SW_f-SPINAL delivering best intensities and concomitant resolution.

The ^{19}F *off-resonance* effects on decoupling performance are shown in Fig. 3. Here, the decoupler frequency was deliberately moved away from the position judged to best represent *on-resonance*. (A good criterion for *on-resonance* condition is to take the maximum of the parabolic intensity curve displayed by ^{13}C on changing the ^{19}F frequency [29].) The *off-resonance* effects were more prominent in NFBS-K than in PFP-Na, and therefore the former is used here-onwards for the discussion. The comparison of decoupling efficiencies of the various methods was done through the analysis of ^{13}C intensities of the CF_2 and CF_3 resonances of NFBS-K. In Fig. 3, the response of the different carbon atoms in NFBS-K to changing the ^{19}F frequency offset by ±12 kHz is shown. Plotted are the data for the three CF_2 carbons (α, β and γ) and the CF_3 carbon (δ), acquired at 10 kHz MAS frequency. It can be seen from Fig. 3 that small offset changes do not have much effect, probably due to the large ^{19}F shielding anisotropy and the presence of homonuclear couplings. The intensity of the carbons β, γ and δ shows the expected parabolic dependence [29], even though the curvature is only weak. For all data, the frequency-swept sequences outperform SPINAL and TPPM by a consistent margin.

The dependence of decoupling efficiency as a function of MAS frequency was also explored. The results are shown in Fig. 4 for all four ^{13}C signals of NFBS-K under *on-resonance* conditions. Here, we plot the full-width-half-height of the ^{13}C lines, instead of the intensities used in all other plots. This was done to exclude possible variations of cross-polarization efficiency with changed MAS, which would affect the intensities. The parameters of the decoupling sequences were optimized at 10 kHz MAS and then kept unchanged for the higher MAS frequencies. It can be seen from Fig. 4 that SW_f-TPPM and SW_f-SPINAL sequences outperform TPPM and SPINAL over all the spinning frequencies analyzed, for the (a) α, (b) δ, (c) β and (d) γ-carbons. The relation between MAS frequency and decoupling efficiency will be discussed in more detail below, in the context of numerical simulation results.

3.2. Numerical simulations using SPINEVOLUTION

The line intensities resulting from the experimentally best-performing SW_f-SPINAL and SW_f-TPPM decoupling sequences were also evaluated by numerical simulations with the SPINEVOLUTION [79] program. The 2D landscapes shown in Fig. 5 portray the absolute intensity of the ^{13}C signal, from a system of a carbon-13 nucleus dipolar-coupled with four ^{19}F nuclei. For the fluorines, a CSA ($\Delta\delta$) of 16 kHz and a dispersion of ^{19}F chemical shifts ($d\delta_{iso}$) of 30 kHz were assumed (see Section 2 for more calculation details). The ^{13}C signal intensity is shown as a function of the *RF* strength (ν_1) applied and the phase angles (ϕ) used. In Fig. 5c, it may be seen that the SW_f-TPPM sequence produces a series of

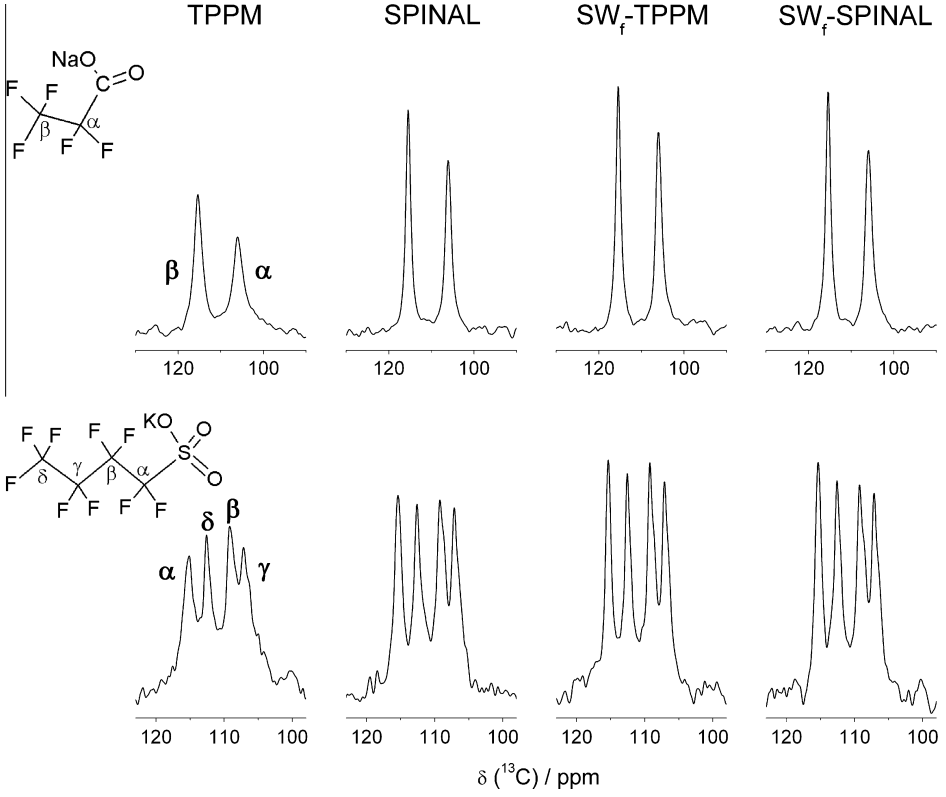

Fig. 2. ^{19}F decoupled ^{13}C CPMAS spectra of (top row) CF_2 and CF_3 groups of sodium pentafluoropropionate (PFP-Na) and (bottom row) potassium nonafluoro-1-butanesulfonate (NFBS-K). Decoupling performance of TPPM, SPINAL, SW_f-TPPM and SW_f-SPINAL are compared for both model compounds. All the spectra were collected at an MAS frequency of 10 kHz, with the decoupler frequency being *on-resonance*.

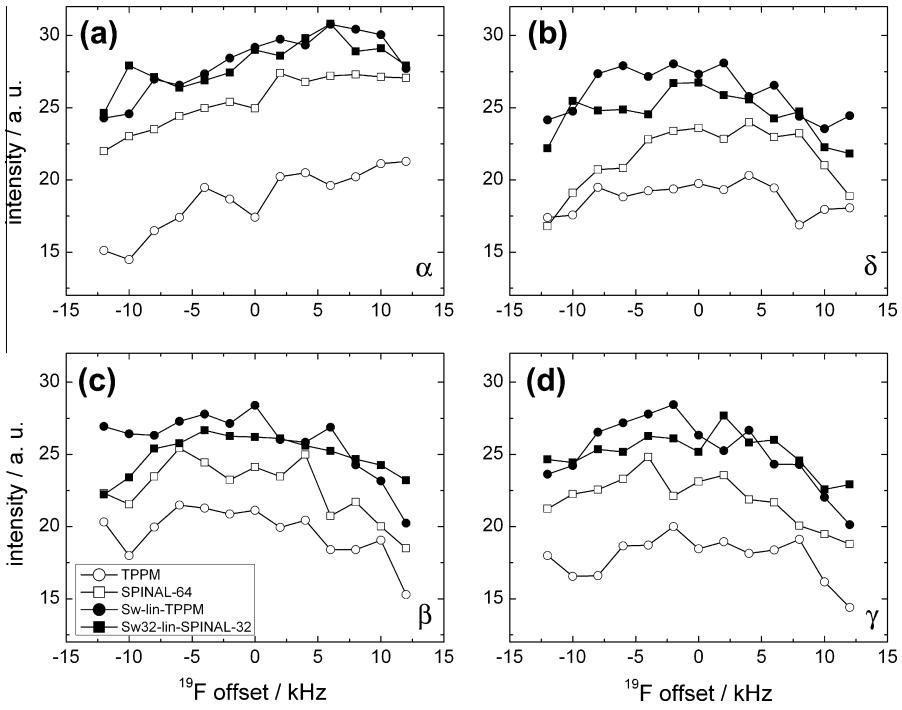

Fig. 3. The ^{19}F *off-resonance* effects are shown for the ^{13}C CPMAS spectra of NFBS-K for the signals from (a) α, (b) δ, (c) β and (d) γ-carbons. Decoupling performance of TPPM, SPINAL, SW$_f$-TPPM and SW$_f$-SPINAL are compared based on the ^{19}F offset dependence at a MAS frequency of 10 kHz.

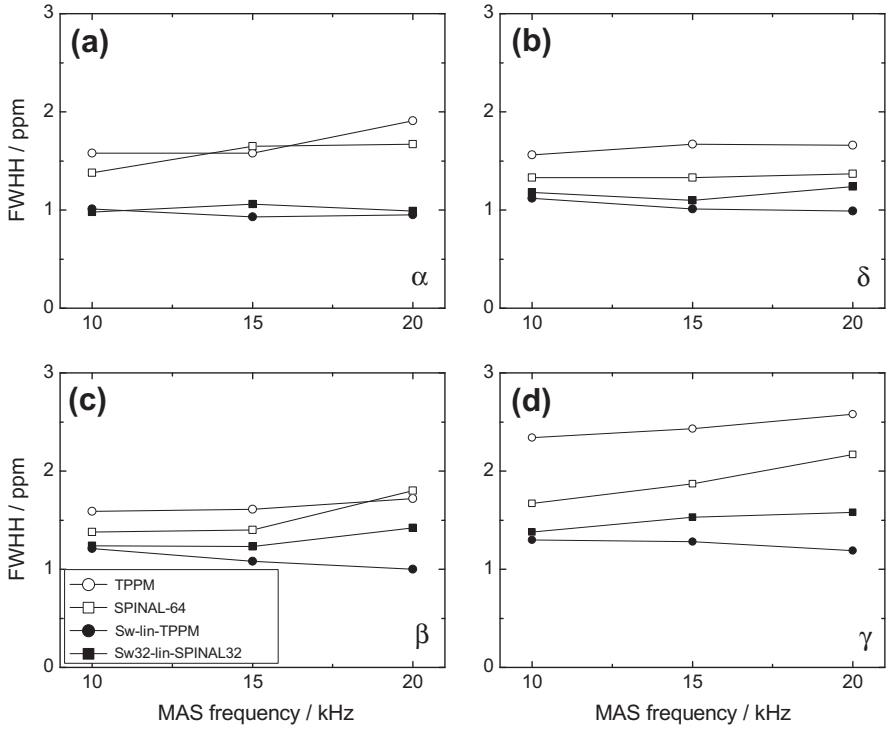

Fig. 4. The decoupling performance at different MAS frequencies are compared here by plotting the full-width-half-height (FWHH) of the ^{13}C CPMAS signals from (a) α, (b) δ, (c) β and (d) γ-carbons of NFBS-K for different decoupling sequences, namely TPPM, SPINAL, SW$_f$-TPPM and SW$_f$-SPINAL at 10, 15 and 20 kHz MAS. Here, in contrast to intensity plots, lower values (i.e., narrower lines) indicate better decoupling.

vertical high-intensity bands which represent the areas where the so-called *decoupling condition* (see below) is met [20]. The location of these bands in the 2D landscape is determined by the ratio of sequence cycle time and rotor period. For SW$_f$-SPINAL, a large spread of moderately good decoupling conditions is visible (see Fig. 5d), albeit without the pronounced band structure observed for SW$_f$-TPPM. For the sake of comparison, numerical simulations of TPPM (Fig. 5a) and SPINAL-64 (Fig. 5b) on the same system are also presented, which exhibit only comparatively small areas of good decoupling efficiency. Thus, also in numerical simulations, the

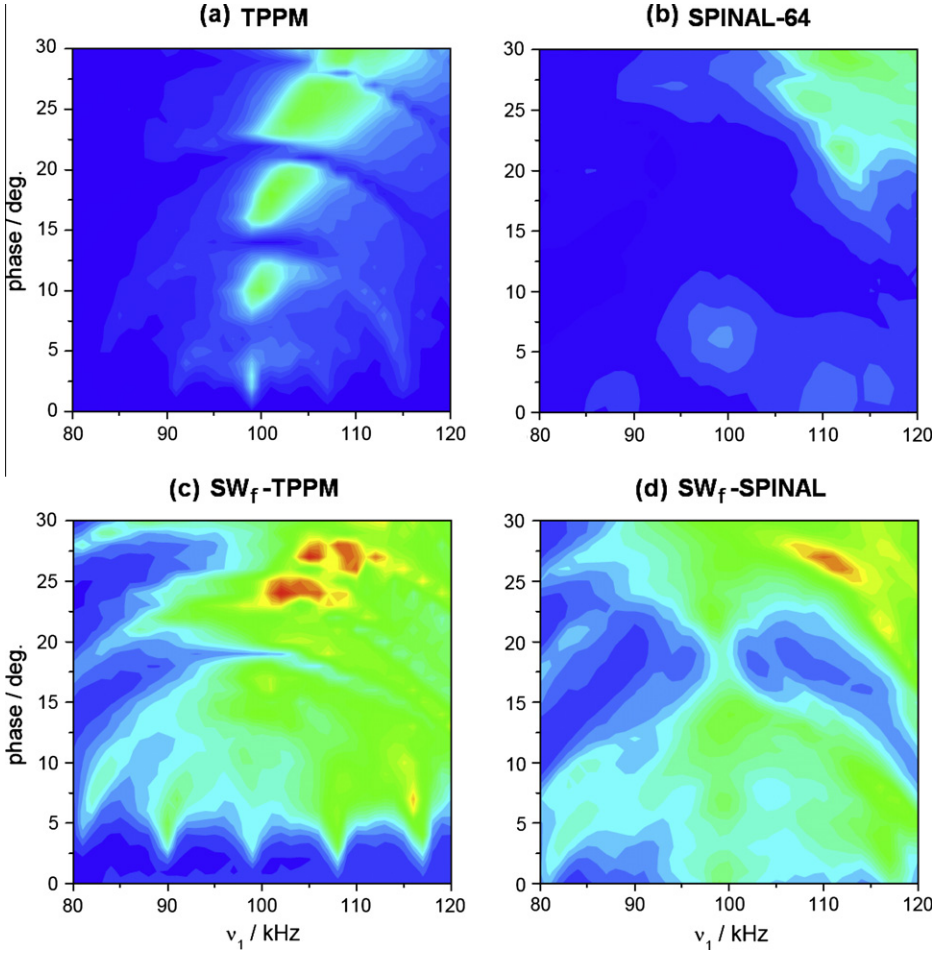

Fig. 5. The 2D representation of SPINEVOLUTION simulations [79] of (a) TPPM, (c) SW_f^{lin}-TPPM (both with 8.0808 kHz MAS); and (b) SPINAL-64, (d) SW_f^{lin}-SPINAL (both with 8.3333 kHz MAS) being plotted as the absolute intensity of the ^{13}C resonance as a function of *RF* strength (ν_1) and the phase angle (ϕ). A structural unit of 4 fluorines (^{19}F, with $\Delta\delta$ = 16 kHz) dipolar-coupled with a ^{13}C ($\Delta\delta$ = 0 kHz) was used for the calculations.

frequency-swept sequences are found to be better performing and more robust than both SPINAL and TPPM.

As explained above, the main difference between decoupling protons or fluorines as abundant spins is the fact that both the chemical shift anisotropy, $\Delta\delta$, and the isotropic dispersion, $d\delta_{iso}$, of ^{19}F is much larger. As in numerical simulations, these parameters may be changed at will, we explored the effect of increasing $\Delta\delta$ for ^{19}F on the decoupling efficiency. In order to do so, full 2D landscapes (such as shown in Fig. 5) were calculated for the investigated decoupling sequences, with the chemical shift anisotropy $\Delta\delta$ of the ^{19}F being varied between 8 and 64 kHz. (By defining the $\Delta\delta$ in kHz, the results are rendered independent of the applied magnetic field.) To handle the information of the 2D plots in a concise manner, we plotted both the maximum intensity found over the 2D grid, as well as the normalized overall intensity summed over the entire grid. These quantities were then plotted over the varying $\Delta\delta$, as depicted in Fig. 6. The resulting dependence for both approaches looks very similar (Fig. 6a and b), showing that the effect on maximum and overall intensity are almost identical. Comparing the different sequences, SW_f-TPPM performs best in ^{19}F decoupling, slightly outperforming SW_f-SPINAL, with both being well ahead in performance to SPINAL-64. With increasing $\Delta\delta$, the relative differences between the decoupling sequences diminish. The classification of sequences by performance, however, remains the same and is very much identical to that observed in the case of proton decoupling [27]. So although large ^{19}F chemical shift anisotropy tends to have a deleterious effect on the decoupling efficiency, the frequency-swept methods are always superior to the non-swept multi-pulse decoupling sequences.

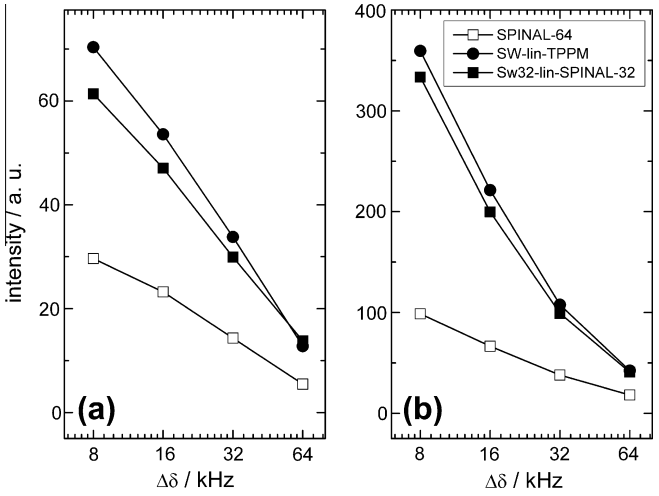

Fig. 6. SPINEVOLUTION [79] simulations showing the decoupling performance of (i) SPINAL-64, (ii) SW_f^{lin}-SPINAL and (iii) SW_f^{lin}-TPPM sequences plotted as a function of (a) the highest intensity values in the 2D plot and (b) the collapsed (summed) intensities of the 2D landscapes, normalized by the matrix size. The decoupling performance was calculated for different chemical shielding anisotropies, $\Delta\delta$ = 8, 16, 32, and 64 kHz.

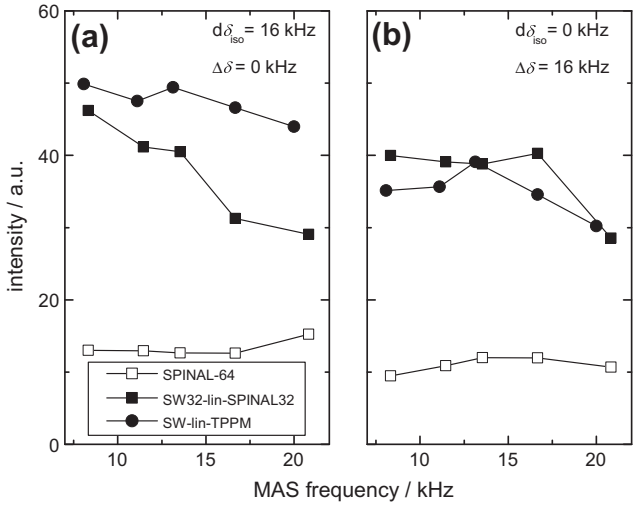

Fig. 7. SPINEVOLUTION [79] simulations showing the decoupling performance of SPINAL-64, SW_f^{lin}-SPINAL and SW_f^{lin}-TPPM sequences plotted as a function of the collapsed (summed) intensities of the 2D landscapes of phase angles (ϕ) and *RF* strengths (ν_1) normalized by the matrix size. The ^{19}F parameters for the four fluorine in the structural units were: (a) $\Delta\delta$ = 0 kHz; $d\delta_{iso}$ = 16 kHz (with δ_{iso} = −8, −8, +8, +8 kHz) and (b) $\Delta\delta$ = 16 kHz; $d\delta_{iso}$ = 0 kHz (with δ_{iso} = 0, 0, 0, 0 kHz). The exact MAS frequencies used were 8.0808, 11.1111, 13.1313, 16.6666 and 20.0000 kHz for SW_f^{lin}-TPPM simulations, while for SPINAL-64 and SW_f^{lin}-SPINAL those were 8.3333, 11.4583, 13.5415, 16.6666 and 20.8333 kHz , to avoid interference effects of τ_c and τ_r.

The main effect of the chemical shift tensor of the abundant nuclei (e.g., ^{19}F) on the linewidth of the observed nuclei (e.g., ^{13}C) is known to be the second-order cross term between chemical shift and heteronuclear dipolar coupling [1,20,80,81]. The numerical simulation results shown in Fig. 6 are consistent with the concept of this cross term being the dominant contribution to the residual linewidth. With increasing $\Delta\delta$ (and correspondingly larger cross-term magnitude), the ^{13}C lines are broadening. In the Floquet analysis of Ref. [20], this cross term can be assigned to an effective Hamiltonian, which possesses a residual field component along the (arbitrarily chosen) *y*-direction. The *decoupling condition* mentioned above is then defined as follows: The effect of the applied decoupling sequence must be such as to eliminate the I_y coefficients of this effective Hamiltonian. For the TPPM and SPINAL sequences, the regime where the decoupling condition is met was shown to be fairly narrow [20]. The frequency sweep performed by the SW_f-TPPM sequence, however, widens the region where the decoupling condition holds [20], which accounts for the improved decoupling performance.

The second-order cross term between the chemical shift and heteronuclear dipolar coupling tensors consists of a sum of a zeroth-rank, a second-rank and a fourth-rank tensor [80], and only the second-rank contribution can be averaged out by MAS rotation. Thus, similar to the isotropic shift dispersion, which is entirely unaffected by MAS, the deleterious effect of the ^{19}F shift anisotropy on the linewidth should not disappear even at faster MAS. This is evident from Fig. 7, where we investigated the influence of $\Delta\delta$ and $d\delta_{iso}$ on the decoupling efficiency. For an assumed chemical shift anisotropy of $\Delta\delta$ = 16 kHz, no beneficial effects of MAS can be observed even at 20 kHz spinning (cf. Fig. 7b). This again points to the fact that the main effect of the chemical shift anisotropy on the residual ^{13}C linewidth is *via* the second-order cross term [1,20,80,81].

4. Conclusions

In this work, we have systematically compared different methods for decoupling ^{19}F in rigid organic solids, with a special emphasis on the recently introduced frequency-swept sequences. Most of the existing heteronuclear spin decoupling pulse sequences in solid-state NMR have been designed and applied for irradiating ^{1}H as the abundant nucleus. However, decoupling of ^{19}F spins is especially demanding due to the existence of large chemical shift effects. For the comparison, an extensive series of NMR experiments at different MAS frequencies on fluorinated model compounds, as well as large sets of numerical simulations were carried out.

From both experiments and simulations it can be concluded that the frequency-swept sequences SW_f-TPPM [18] and SW_f-SPINAL [27] deliver better and more robust spin decoupling than the original sequences SPINAL and TPPM. Although the existence of a large chemical shift anisotropy ($\Delta\delta$) and isotropic dispersion ($d\delta_{iso}$) for ^{19}F does compromise the decoupling efficiency, the relative performance hierarchy of the sequences remains unaffected. From our numerical simulations of decoupling efficiency for increasing $\Delta\delta$, it can be seen that the deleterious effect of the ^{19}F shift anisotropy on the ^{13}C linewidth does not disappear even at faster MAS. This can be attributed to the previously described presence of a second-order cross term between chemical shift and dipolar coupling, which averages only partly under MAS [80]. Similarly, the isotropic shift dispersion $d\delta_{iso}$ is entirely unaffected by MAS rotation. Since the size of $d\delta_{iso}$ is roughly a magnitude smaller than that of $\Delta\delta$ for ^{19}F, the anisotropy $\Delta\delta$ is expected to have overall larger influence on the decoupling performance.

In summary, for NMR of fluorine-containing rigid organic solids under moderate MAS conditions ($\leqslant$20 kHz), decoupling sequences that work well for proton decoupling should also exhibit good performance for fluorine decoupling.

Acknowledgments

Financial support by Deutsche Forschungsgemeinschaft (Grant BR 3370/4-1) is gratefully acknowledged. The authors would like to thank R.S. Thakur (CSMCRI, Gujarat) for useful discussions. We also thank K. Saalwächter (MLU Halle) for spectrometer time and support.

References

[1] M. Ernst, Heteronuclear spin decoupling in solid-state NMR under magic-angle sample spinning, J. Magn. Reson. 162 (2003) 1–34.
[2] P. Hodgkinson, Heteronuclear decoupling in the NMR of solids, Prog. Nucl. Magn. Reson. Spectrosc. 46 (2005) 197–222.
[3] A.L. Bloom, J.N. Shoolery, Effects of perturbing radiofrequency fields on nuclear spin coupling, Phys. Rev. 97 (1955) 1261–1265.
[4] F. Bloch, Theory of line narrowing by double-frequency irradiation, Phys. Rev. 111 (1958) 841–853.
[5] L.R. Sarles, R.M. Cotts, Double nuclear magnetic resonance and the dipole interaction in solids, Phys. Rev. 111 (1958) 853–859.
[6] A.E. Bennett, C.M. Rienstra, M. Auger, K.V. Lakshmi, R.G. Griffin, Heteronuclear decoupling in rotating solids, J. Chem. Phys. 103 (1995) 6951–6958.
[7] B.M. Fung, A.K. Khitrin, K. Ermolaev, An improved broadband decoupling for liquid crystals and solids, J. Magn. Reson. 142 (2000) 97–101.
[8] T. Bräuniger, P. Wormald, P. Hodgkinson, Improved proton decoupling in NMR spectroscopy of crystalline solids using the SPINAL-64 sequence, Monatsh. Chem. 133 (2002) 1549–1554.
[9] G. de Paëpe, A. Lesage, L. Emsley, The performance of phase modulated heteronuclear dipolar decoupling schemes in fast magic-angle-spinning nuclear magnetic resonance experiments, J. Chem. Phys. 119 (2003) 4833–4841.
[10] A. Detken, E.H. Hardy, M. Ernst, B.H. Meier, Simple and efficient decoupling in magic-angle spinning solid-state NMR: the XiX scheme, Chem. Phys. Lett. 356 (2002) 298–304.
[11] P. Tekely, P. Palmas, D. Canet, Phase-modulated irradiation for efficient heteronuclear decoupling in rapidly rotating solids, J. Magn. Reson. A107 (1994) 129–133.
[12] M. Eden, M.H. Levitt, Pulse sequence symmetries in the nuclear magnetic resonance of spinning solids: application to heteronuclear decoupling, J. Chem. Phys. 111 (1999) 1511–1519.

[13] J. Leppert, O. Ohlenschläger, M. Görlach, R. Ramachandran, Adiabatic heteronuclear decoupling in rotating solids, J. Biomol. NMR 29 (2004) 319–324.
[14] G.D. Paëpe, B. Elèna, L. Emsley, Characterization of heteronuclear decoupling through proton spin dynamics in solid-state nuclear magnetic resonance spectroscopy, J. Chem. Phys. 121 (2004) 3165–3180.
[15] X. Filip, C. Tripon, C. Filip, Heteronuclear decoupling under fast MAS by a rotor-synchronized Hahn-echo pulse train, J. Magn. Reson. 176 (2005) 239–243.
[16] R. Fu, Efficient heteronuclear dipolar decoupling in NMR of static solid sample using phase-wiggled two-pulse phase modulation, Chem. Phys. Lett. 483 (2009) 147–153.
[17] I. Scholz, P. Hodgkinson, B.H. Meier, M. Ernst, Understanding two-pulse phase-modulated decoupling in solid-state NMR, J. Chem. Phys. 130 (2009) 114510.
[18] R.S. Thakur, N.D. Kurur, P.K. Madhu, Swept-frequency two-pulse phase modulation for heteronuclear dipolar decoupling in solid-state NMR, Chem. Phys. Lett. 426 (2006) 459–463.
[19] R.S. Thakur, N.D. Kurur, P.K. Madhu, Improved heteronuclear dipolar decoupling sequences for liquid–crystal NMR, J. Magn. Reson. 185 (2007) 264–269.
[20] M. Leskes, R.S. Thakur, P.K. Madhu, N.D. Kurur, S. Vega, Bimodal Floquet description of heteronuclear dipolar decoupling in solid-state nuclear magnetic resonance, J. Chem. Phys. 127 (2007) 024501.
[21] R.S. Thakur, N.D. Kurur, P.K. Madhu, An experimental study of decoupling sequences for multiple-quantum and high-resolution MAS experiments in solid-state NMR, Magn. Reson. Chem. 46 (2008) 166–169.
[22] C.V. Chandran, P.K. Madhu, N.D. Kurur, T. Bräuniger, Swept-frequency two-pulse phase modulation (SW_f-TPPM) sequences with linear sweep profile for heteronuclear decoupling in solid-state NMR, Magn. Reson. Chem. 46 (2008) 943–947.
[23] R.S. Thakur, N.D. Kurur, P.K. Madhu, An analysis of phase-modulated heteronuclear dipolar decoupling sequences in solid-state nuclear magnetic resonance, J. Magn. Reson. 193 (2008) 77–88.
[24] T. Bräuniger, G. Hempel, P.K. Madhu, Fast amplitude-modulated pulse trains with frequency sweep (SW-FAM) in static NMR of half-integer spin quadrupolar nuclei, J. Magn. Reson. 181 (2006) 68–78.
[25] C.V. Chandran, J. Cuny, R. Gautier, L. Le Pollès, C.J. Pickard, T. Bräuniger, Improving sensitivity and resolution of MQMAS spectra: a ^{45}Sc-NMR case study of scandium sulphate pentahydrate, J. Magn. Reson. 203 (2010) 226–235.
[26] R.S. Thakur, N.D. Kurur, P.K. Madhu, Pulse duration and phase modulated heteronuclear dipolar decoupling schemes in solid-state NMR, In: Sp. Ed. Proc. Indian Natl. Sci. Acad., Springer-Verlag, in press.
[27] C.V. Chandran, T. Bräuniger, Efficient heteronuclear dipolar decoupling in solid-state NMR using frequency-swept SPINAL sequences, J. Magn. Reson. 200 (2009) 226–232.
[28] E. Brunner, D. Fenzke, D. Freude, H. Pfeifer, The influence of homonuclear dipolar interaction on the residual linewidths of MAS NMR spectra, Chem. Phys. Lett. 169 (1990) 591–594.
[29] D.L. VanderHart, G.C. Campbell, Off-resonance proton decoupling on-resonance and near-resonance, J. Magn. Reson. 134 (1998) 88–112.
[30] J. Mason, Conventions for the reporting of nuclear magnetic shielding (or shift) tensors suggested by participants in the NATO ARW on NMR shielding constants at the University of Maryland, College Park, July 1992, Solid State Nucl. Magn. Reson. 2 (1993) 285–288.
[31] J. Vaara, K. Oikarinen, J. Jokisaari, J. Lounila, Anisotropy of the ^{1}H and ^{13}C shielding tensors in chloroform, Chem. Phys. Lett. 253 (1996) 340–348.
[32] B.R. Appleman, B.P. Dailey, Fluorine shielding anisotropy in $CFCl_3$, J. Magn. Reson. 16 (1974) 265–273.
[33] S.G. Kukolich, Proton magnetic shielding tensors from spin-rotation measurements on H_2CO and NH_3, J. Am. Chem. Soc. 97 (1975) 5704–5707.
[34] T. Kupka, B. Ruscic, R.E. Botto, Hartree–Fock and density functional complete basis-set (CBS) predicted nuclear shielding anisotropy and shielding tensor components, Solid State Nucl. Magn. Reson. 23 (2003) 145–167.
[35] M.R. Baker, C.H. Anderson, N.F. Ramsey, Nuclear magnetic resonance antishielding of nuclei in molecules. Magnetic moments of ^{19}F, ^{14}N and ^{15}N, Phys. Rev. 133 (1964) A1533–1536.
[36] A.B. Harris, E. Hunt, H. Mayer, Anisotropy of the ^{19}F chemical shift of trapped CHF_3 and NF_3, J. Chem. Phys. 42 (1965) 2851–2862.
[37] C. Coupry, M.-T. Chenon, L.G. Werbelow, ^{13}C nuclear magnetic resonance study of the solution-state dynamics of benzene, J. Chem. Phys. 101 (1994) 899–904.
[38] M. Mehring, R.G. Griffin, J.S. Waugh, ^{19}F shielding tensors from coherently narrowed NMR powder spectra, J. Chem. Phys. 55 (1971) 746–755.
[39] C.S. Yannoni, B.P. Dailey, G.P. Ceasar, Studies of chemical shift anisotropy in liquid crystal solvents. IV. Results for some fluorine compounds, J. Chem. Phys. 54 (1971) 4020–4023.
[40] T.K. Halstead, H.W. Spiess, U. Haeberlen, ^{19}F and ^{1}H shielding tensors and crystal structure of 4,4′-difluorobiphenyl, Mol. Phys. 31 (1976) 1569–1583.
[41] K. Dorai, A. Kumar, Fluorine chemical shift tensors in substituted fluorobenzenes using cross correlations in NMR relaxation, Chem. Phys. Lett. 335 (2001) 176–182.
[42] T. Schaller, D.B. Dingwell, H. Keppler, W. Knöller, L. Merwin, A. Sebald, Fluorine in silicate glasses: a multinuclear nuclear magnetic resonance study, Geochim. Cosmochim. Acta 56 (1992) 701–707.
[43] E.W. Hagaman, ^{13}C–^{19}F dipolar dephasing in monofluorinated organic substances. Characterization by ^{1}H–^{13}C–^{19}F triple-resonance ^{13}C CP/MAS and ^{19}F MAS NMR, J. Magn. Reson. 104A (1993) 125–131.
[44] M. Pruski, D.P. Lang, C. Fernandez, J.P. Amoureux, Multiple-quantum magic-angle spinning NMR with cross-polarization: spectral editing of high-resolution spectra of quadrupolar nuclei, Solid State Nucl. Magn. Reson. 7 (1997) 327–331.
[45] B. Bureau, G. Silly, J.Y. Buzaré, CP-MAS ^{207}Pb with ^{19}F decoupling NMR spectroscopy: medium range investigation in fluoride materials, Solid State Nucl. Magn. Reson. 15 (1999) 79–89.
[46] P. Bertani, J. Raya, P. Reinheimer, R. Gougeon, L. Delmotte, J. Hirschinger, ^{19}F/^{29}Si distance determination on fluoride-containing octadecasil by Hartmann–Hahn cross-polarization under fast magic-angle spinning, Solid State Nucl. Magn. Reson. 13 (1999) 219–229.
[47] J.C.C. Chan, H. Eckert, High-resolution ^{27}Al–^{19}F solid-state double resonance NMR studies of AlF_3–BaF_2–CaF_2 glasses, J. Non-Cryst. Solids 284 (2001) 16–21.
[48] G. Scholz, O. Korup, High-energy ball milling – a possible synthesis route for cryolite and chiolite, Solid State Sci. 8 (2006) 678–684.
[49] J. Giraudet, M. Dubois, K. Guérin, A. Hamwi, F. Masin, Solid state NMR studies of covalent graphite fluorides $(CF)_n$ and $(C_2F)_n$, J. Phys. Chem. Solids 67 (2006) 1100–1105.
[50] L. Zhang, C.C. de Araujo, H. Eckert, Structural role of fluoride in aluminophosphate sol–gel glasses: high-resolution double-resonance NMR studies, J. Phys. Chem. B 111 (2007) 10402–10412.
[51] J. Giraudet, M. Dubois, K. Guérin, C. Delabarre, P. Pirotte, A. Hamwi, F. Masin, Heteronuclear dipolar recoupling using Hartmann–Hahn cross polarization: a probe for ^{19}F–^{13}C distance determination of fluorinated carbon materials, Solid State Nucl. Magn. Reson. 31 (2007) 131–140.
[52] F.J. Berry, E. Moore, M. Mortimer, X. Ren, R. Heap, P. Slater, M.F. Thomas, Synthesis and structural investigation of a new oxide fluoride of composition $Ba_2SnO_{2.5}F_3{\cdot}xH_2O$ ($x \approx 0.5$), J. Solid State Chem. 181 (2008) 2185–2190.
[53] C. Serre, M. Haouas, F. Taulelle, W. Van Beek, G. Férey, Synthesis, structure and solid state NMR analysis of new templated titanium (III/IV) fluorophosphate, C. R. Chim. 13 (2010) 336–342.
[54] S.V. Dvinskikh, R. Sitnikov, I. Furó, ^{13}C PGSE NMR experiment with heteronuclear dipolar decoupling to measure diffusion in liquid crystals and solids, J. Magn. Reson. 142 (2000) 102–110.
[55] G. Silly, C. Legein, J.Y. Buzaré, F. Calvayrac, Electric field gradients in fluoride crystalline powders: correlation of NMR measurements with ab initio calculations, Solid State Nucl. Magn. Reson. 25 (2004) 241–251.
[56] M. Gerken, P. Hazendonk, J. Nieboer, G.J. Schrobilgen, NMR spectroscopic study of xenon fluorides in the gas phase and of XeF_2 in the solid state, J. Fluorine Chem. 125 (2004) 1163–1168.
[57] P. Florian, E.M. Anghel, C. Bessada, Structured description of the $Na_2B_4O_7$–Na_3AlF_6–TiO_2 system. 2. A multinuclear NMR approach of melts and solids, J. Phys. Chem. B 111 (2007) 968–978.
[58] A. Pawlik, R. König, G. Scholz, E. Kemnitz, G. Brunklaus, M. Bertmer, C. Jäger, Access to local structures of HS–AlF_3 and its precursor determined by high-resolution solid-state NMR, J. Phys. Chem. C 113 (2009) 16674–16680.
[59] P.K. Pallathadka, S.S. Tay, L. Tinaxi, P. Sprenger, Solid state ^{19}F NMR study of crystal transformation in PVDF and its nanocomposites, Polym. Sci. Eng. 46 (2006) 1684–1690.
[60] N.G. Karpukhina, U. W- Zwanziger, J.W. Zwanziger, A.A. Kiprianov, Preferential binding of fluorine to aluminium in high peralkaline aluminosilicate glasses, J. Phys. Chem. B 111 (2007) 10413–10420.
[61] S. Hoyer, T. Emmler, K. Seppelt, The structure of xenon hexafluoride in solid state, J. Fluorine Chem. 127 (2006) 1415–1422.
[62] B. Zhou, B.L. Sherriff, J.S. Hartman, G. Wu, ^{27}Al and ^{23}Na NMR spectroscopy and structural modeling of aluminofluoride minerals, Am. Mineral. 92 (2007) 34–43.
[63] G. Antonioli, D.E. McMillan, P. Hodgkinson, Line-splitting and broadening effects from ^{19}F in the ^{13}C NMR of liquid crystals and solids, Chem. Phys. Lett. 344 (2001) 68–74.
[64] J.C. Cherryman, R.K. Harris, New multinuclear experiments on solid organotin fluorides, J. Magn. Reson. 128 (1997) 21–29.
[65] A. Nordon, R.K. Harris, L. Yeo, K.D.M. Harris, Application of triple-channel ^{13}C{^{1}H,^{19}F} NMR techniques to probe structural properties of disordered solids, Chem. Commun. 33 (1997) 2045–2046.
[66] R.K. Harris, A. Nordon, K.D.M. Harris, Ring inversion of fluorocyclohexane in its solid thiourea inclusion compound, Magn. Reson. Chem. 37 (1999) 15–24.
[67] R.K. Harris, L.A. Crowe, Solid-state NMR studies of fluorinated diazadiphosphetidines, J. Chem. Soc. Dalton Trans. 28 (1999) 4315–4323.
[68] M. Bechmann, K. Hain, C. Marichal, A. Sebald, X-{^{1}H, ^{19}F} triple resonance with a X-{^{1}H} CP MAS probe and characterisation of a ^{29}Si–^{19}F spin pair, Solid State Nucl. Magn. Reson. 23 (2003) 50–61.
[69] X. Helluy, R. Pietschnig, A. Sebald, ^{29}Si and ^{19}F MAS NMR spectra of isolated ^{29}Si(^{19}F)$_2$ and ^{29}Si(^{19}F)$_3$ spin systems: experiments and simulations, Solid State Nucl. Magn. Reson. 24 (2003) 286–300.
[70] J.P. Donoso, T.J. Bonagamba, P.L. Frare, N.C. Mello, C.J. Magon, H. Panepucci, Nuclear magnetic relaxation study of poly(propylene oxide) complexed with lithium salt, Electrochim. Acta 40 (1995) 2361–2363.
[71] P. Holstein, U. Scheler, R.K. Harris, Triple-channel solid-state NMR investigation of poly(vinylidene fluoride) polymorphs, Magn. Reson. Chem. 35 (1997) 647–649.
[72] S.-F. Liu, K. Schmidt-Rohr, High-resolution solid-state ^{13}C NMR of fluoropolymers, Macromolecules 34 (2001) 8416–8418.
[73] J.S. Forsythe, D.J.T. Hill, A.K. Wittaker, The use of NMR for determination of new structures in irradiated TFE/PMVE fluoropolymers, Radiat. Phys. Chem. 60 (2001) 609–615.

[74] P. Hazendonk, C. deDenus, A. Iuga, P. Cahoon, B. Nilsson, D. Iuga, A morphological study of poly[bis(trifluoroethoxy)phosphazene] using solid-state NMR: introducing domain selective ^{1}H and ^{19}F decoupled ^{13}C MAS NMR, J. Inorg. Organomet. Polym. Mater. 16 (2006) 343–357.
[75] Q. Chen, K. Schmidt-Rohr, Backbone dynamics of the nafion ionomer studied by ^{19}F–^{13}C solid-state NMR, Macromol. Chem. Phys. 208 (2007) 2189–2203.
[76] P. Wormald, B. Ameduri, R.K. Harris, P. Hazendonk, High-resolution ^{19}F and ^{1}H NMR of a vinylidenefluoride telomer, Polymer 49 (2008) 3629–3638.
[77] M. Weingarth, P. Tekely, G. Bodenhausen, Efficient heteronuclear decoupling by quenching rotary resonance in solid-state NMR, Chem. Phys. Lett. 466 (2008) 247–251.
[78] M. Weingarth, G. Bodenhausen, P. Tekely, Low-power decoupling at high spinning frequencies in high static fields, J. Magn. Reson. 199 (2009) 238–241.
[79] M. Veshtort, R.G. Griffin, SPINEVOLUTION: a powerful tool for the simulation of solid and liquid state NMR experiments, J. Magn. Reson. 178 (2006) 248–282.
[80] M. Ernst, S. Bush, A.C. Kolbert, A. Pines, Second-order recoupling of chemical-shielding and dipolar-coupling tensors under spin decoupling in solid-state NMR, J. Chem. Phys. 105 (1996) 3387–3397.
[81] D.B. Zax, Field-dependent isotropic shifts and limitations to linewidths in solid state nuclear magnetic resonance: a Floquet treatment, J. Chem. Phys. 105 (1996) 6616–6625.